THE BASIN-IMPACTOR DEBRIS MODEL FOR THE ORIGIN OF THE LATE HEAVY BOMBARDMENT. P. H. Schultz, Department of Earth, Environmental and Planetary Sciences, Brown University, 324 Brook St, Box 1846, Providence, RI, 02912; peter_schultz@brown.edu.

Introduction: Background: Both lunar sample ages and crater statistics indicate that the inner planets experienced a period of heavy bombardment (LHB) well after accretion. In crater statistics, the LHB is expressed as a departure from a simple power-law distribution in the size versus number-density in the lunar highlands. This departure could be interpreted in three ways: (a) an excess of craters between 20 km and 100 km indicating a late supply of 1 km -10 km diameter bodies [1]; (b) removal of craters smaller than about 50 km through re-surfacing [2; 3]; or (c) a depletion of objects greater than 70 km in diameter [4]. Explanations for the sudden supply, source region, and population of the bodies responsible for the LHB almost 0.5 Ga after the formation of the Moon include: dynamical stirring of the asteroid belt by the formation and/or orbital evolution of the giant planets leading to a cascade of bodies over 0.3 Ga [5,6]; a much shorter cataclysmic spike in debris [7,8], perhaps from delayed disruption of a 5th planet [9]; or debris ejected from large-body collisions [10,11].

Here we explore the hypothesis that the LHB could reflect the sudden supply of impactor debris escaping large oblique basin-forming collisions, i.e., a *Basin Impactor Debris* (*BID*) model [10; 11]. Rather than a single mega-basin, such as debris from proposed Borealis Basin on Mars [4], this model argues that significant mass fractions (>50%) of the projectile survive modestly oblique asteroidal collisions responsible for some of the established large Nectarian and Imbrian impact basins. After disruption and escaping the initial collision, their planet-crossing orbits return to generate the observed LHB. In order to test this hypothesis, laboratory experiments were performed at the NASA Ames Vertical Gun Range. While small in scale, such experiments demonstrate that the same basic physics also apply at much larger scales (through hydrocodes) and reveal processes that can be used to guide and constrain new models.

Laboratory Experiments: Aluminum spheres (0.635 cm diameter) impacted a 6.35 cm aluminum cylinder (6061) from 3 km/s to 5.5 km/s at impact angles from 5° to 35° with respect to the tangent plane at the point of impact. For simplicity, aluminum was used for both target and projectiles (matched impedance). A subset of rounds, however, assessed the effect of low-impedance layers (½ to ¼ the projectile diameter of plasticene) on projectile disruption. Multiple cameras recorded each event from different viewpoints: high-speed color stereo imaging of the collision from the side (>100 kfps); high-speed (500 kfps) black and white camera focused on the impact point from above; and another (125 kfps) on a witness plate about 1 m downrange. Imaging of this plate timed debris arrival (hence speed) and captured the evolving pattern (and trajectories). Craters on the plate were then used to calculate the size of the impacting debris from well-determined crater-scaling relations. Another series of experiments used back lighting in order to capture the debris in flight.

Results: Stereo imaging at the impact point captured the evolving distribution of emerging debris from the projectile (Fig. 1). A plane of fine debris traveling at ~ 10 km/s trails behind the leading jetting phase (15 km/s – 20 km/s). A larger cloud of debris emerges as the optical depth of the plasma increases and forms a downward-directed, V-shaped pattern with the apex leading downrange. The two sides of the V curve upward, like wings, and trail behind the leading edge. At impact angles *below* 20°, several (1-3) large fragments travel at speeds close to the initial projectile with only a slight deflection (5°–10°) from the original trajectory. For impact angles *above* 20°, the leading debris also travels close (95%) to the initial collision speed but contains 10 similar size fragments. In both cases, the fragments are non-luminous (hence, cool) but are trailed by reddish (warmer) finer debris to either side. Backlit-image sequences confirm that leading fragments impacting the witness plates represent individual fragmental debris with sizes consistent with those derived from the witness plates. Impacts into a thin (1.6 mm) low-impedance layer of plasticene on top of the Al target generated larger debris at (same launch speed), even though the crater on the disc left only a depression in the substrate.

The size distribution of the surviving fragments (from the witness plates) changes dramatically from 25°–30° to 18° impact angles (Fig. 2). For impact angles ~20° at ~3 km/s, the largest fragment is ~ 70% of the original projectile, with the next 4 largest only 2.5 times smaller. At higher impact speeds, one large fragment still dominates but is now slightly smaller (63%) with the next four fragments closer in size. For higher impact angles (20°–30°) at ~3km/s, however, the 5 largest fragments have nearly the same size, ~43%. The size of the largest fragment decreases with increasing speeds at the higher angles: 43% at 3 km/s to 33% at 5.5km/s.

Previous laboratory experiments demonstrate that large fractions of the original projectile survive at the

speeds available in the laboratory and decouple from the target for impact angles up to 10° [13]. On curved surfaces, however, decoupling can occur at angles up to 20° (here, a diameter ratio of 10:1). Computational models using CTH [11; 12] reveal the same basic pattern of survival. Analyses of basins on the Moon document grooves [14] that exhibit the same pattern of downrange debris from the impactor (rather than lunar debris). Hence, processes observed in the experiments do apply (with caveats) at much larger scales.

Implications: Based on these results, large oblique impacts should generate significant decoupled projectile debris from mega-basin formation (e.g., SPA) and multiple-fragmented debris from large basins (e.g., Imbrium, Crisium, Orientale). If only 1/3 of the initial mass from a 700 km (SPA scale) in diameter oblique collision (~20° – 30°) survives, the largest debris represents 0.0001% of the initial mass and would release 300,000 fragments with sizes up to 7 km in diameter (producing 100 km diameter craters). For a smaller size (250 km) Imbrium-size impactor, the same fraction would generate a similar number of 2.5 km diameter fragments (producing 20-50 km diameter craters). In the *BID* model, the LHB may be a record of returning debris from a few large basin-forming impacts by large (100 km to 500 km) asteroids from 4.3 Ga to 3.8 Ga. While focused on the Moon here, the same process would have been ongoing on the Earth (when the Moon was 1/3 to 1/2 its present distance), as well as on all other terrestrial planets and asteroids (e.g., Vesta). While migration of the gas giants dynamically ejected objects out of the original asteroid belt, it is suggested that they disturbed larger proto-planets responsible for the large basins and the debris that produced the excess in 10 km-100 km craters. Moreover, the present size of the bodies in the asteroid belt may be survivors of such collisions, rather than a reflection of an original population [1]. As a result, the LHB may represent short-duration spikes in crater-formation rates after each oblique basin-forming collision. Crater statistics during this time, therefore, could only be used for relative time, not a uniform cratering rate.

References: [1] Strom, R. G. (2005), *Science* 309, 1847-1850; [2] Hartmann, W. K. (1975), *Icarus* 247-263; [3] Chapman *et al*. (2002), *LPSC 33*, 1627; [4] Minton, D. A. *et al.* (2015), Icarus 247, 172-190; [5] Wetherill, G. (1975), *Proc. Lunar Planet. Sci. Conf. 6th*, 1539-1561; [6] Gomes *et al*. (2005), *Nature* 435, 466-469; [7] Ryder, G. (2003), *Eos Trans. AGU* 71, 313–323; [8] Spudis, P. D. *et al.* (2011), *Jour. Geophys. Res.*116, doi: 10.1029/2011JE003903; [9] Chambers, J. E. (2007), *Icarus* 189, 386-400; [10] Schultz, P. H. & Crawford, D. A. (2008), *Workshop on Early Solar System Impact Bombardment*, #3026; [11] Schultz, P. H. & Crawford, D. A. (2011) *Geol. Soc. Sp. Paper* 477, p. 141-159; [12] Schultz P. H. *et al.* (2012), *Lunar Planet. Science 43*, #2428; [13] Schultz, P.H. & Gault, D.E. (1990), *Geol. Soc. Sp. Paper* 247, 239-261; [14] Schultz, P. H. & Crawford, D. A. (2014), *Lunar Planet. Sci. 45*, #1961.

Fig. 1A: Stereo view of surviving projectile fragments (lower left center) passing through the self-luminous plasma generated by a 5.2 km/s sphere impacting a cylinder at 18° from the surface tangent (right). Faint line corresponds to a trajectory of 30° from the impact point. Leading fragments retain travel downrange near the initial impact speed. Faint blue component at left is the jetting phase, which has passed out of the field of view. Heated fine debris (due to frictional shear) trail the cooler fragments at front (lower left).

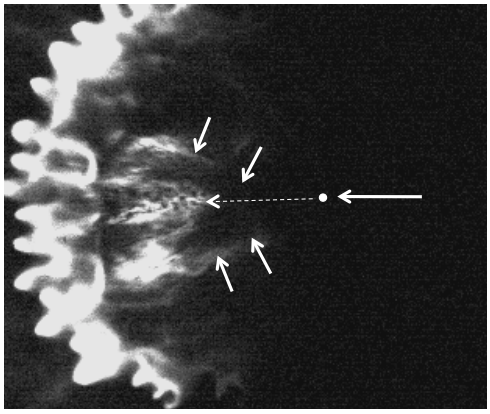

Fig. 1B: Oblique impact of a spherical aluminum projectile into the top of a cylinder (from above). Strings of impactor fragments travel downrange along the initial trajectory (dashed arrow) from the impact point (dot) while finer debris extends to either side (solid arrows). Bright sinuous pattern marks the leading edge of the impact vapor, behind jetting.

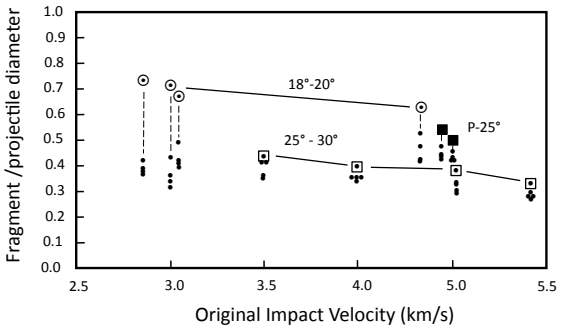

Fig. 3: Sizes of impactor fragments surviving oblique impacts into aluminum cylinders at different speeds and angles. Circled dots indicate the largest fragment from each experiment at lower impact angles; squares with dots, higher angles. Filled squared represent the effect of plasticene (P) layers ¼ (left) and ½ (right) the projectile diameter. Dots indicate the next four largest fragments observed.